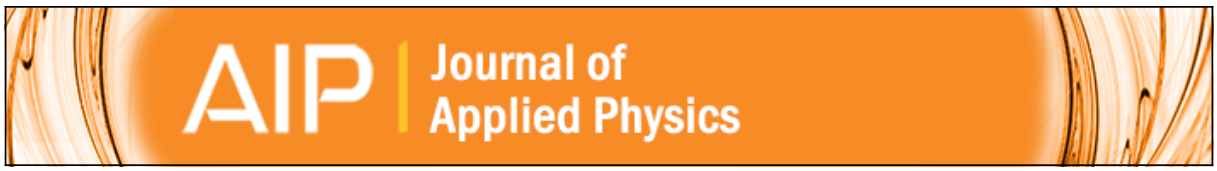

Evidence on simultaneous improvement of motional impedance and Q-factor of silicon phononic crystal micromechanical resonators by variously engineering the cavity defects

Nan Wang, Fu-Li Hsiao, Moorthi Palaniapan, and Chengkuo Lee

Citation: Journal of Applied Physics **115**, 094904 (2014); doi: 10.1063/1.4867044
View online: http://dx.doi.org/10.1063/1.4867044
View Table of Contents: http://scitation.aip.org/content/aip/journal/jap/115/9?ver=pdfcov
Published by the AIP Publishing

[This article is copyrighted as indicated in the article. Reuse of AIP content is subject to the terms at: http://scitation.aip.org/termsconditions. Downloaded to] IP: 137.132.250.14 On: Thu, 06 Mar 2014 06:08:49

Evidence on simultaneous improvement of motional impedance and *Q*-factor of silicon phononic crystal micromechanical resonators by variously engineering the cavity defects

Nan Wang,[1,2] Fu-Li Hsiao,[3] Moorthi Palaniapan,[1] and Chengkuo Lee[1,a)]
[1]*Department of Electrical and Computer Engineering, National University of Singapore, 4 Engineering Drive 3, Singapore 117576*
[2]*Institute of Microelectronics, A*STAR (Agency for Science, Technology and Research), 11 Science Park Road, Singapore Science Park II, Singapore 117685*
[3]*Graduate Institute of Photonics, National Changhua University of Education, No. 1, Jin-De Road, Changhua City 500, Taiwan*

(Received 18 November 2013; accepted 16 February 2014; published online 5 March 2014)

In this work, we report the experimental evidence on the capability to simultaneously improve the *Q*-factor (*Q*) and motional impedance (*Z*) of silicon phononic crystal (PnC) micromechanical (MM) resonators by properly engineering the cavity defects on an otherwise perfect two-dimensional (2D) silicon PnC slab. The cavity defects of the resonators in the current study are engineered by patterning additional scattering holes to the pure Fabry-Perot resonant cavity, which is created by deleting two rows of scattering air holes from the centre of the 2D square air-hole array. Experimental results show that by varying the radii of the additional scattering holes patterned in the cavity, the fabricated silicon PnC MM resonators can have their *Q* and *Z* improved simultaneously, showing great potential in overcoming the trade-off between *Z* and *Q* in conventional resonators of piezoelectric type and capacitive type. © *2014 AIP Publishing LLC*.
[http://dx.doi.org/10.1063/1.4867044]

I. INTRODUCTION

Over the recent years, silicon-based micromechanical (MM) oscillators are gaining intensive research focus due to their compatibility with integrated circuit (IC) process and their potential to replace quartz crystals, which are not IC-compatible, to be the next-generation frequency reference oscillator in the communication devices of radio frequency.[1] However, there is a trade-off between the two mainstream silicon MM resonator approaches, namely, capacitive-type[2–5] and piezoelectric-type[6–8] approaches, which is also known as the trade-off between the *Q*-factor (*Q*) and motional impedance (*Z*). Specifically, for resonators of capacitive type, high *Q* can be obtained which then reduces the complexity of the oscillator IC with high frequency selectivity on one hand. On the other hand, the high Z associated with this type of resonators leads to high power consumption.[9] Whereas for resonators of piezoelectric type, characteristics are the opposite to the capacitive-type resonators, i.e., they have low *Z* of below 50 Ω which reduces the power consumption, however, they have lower *Q* than the capacitive-based devices[10] which increases the IC complexity.

Phononic crystals (PnCs), which are artificially structured materials with periodically varying elastic coefficients, are a type of materials with high potential to overcome the trade-off between the *Q* and *Z* in aforementioned devices of capacitive type and piezoelectric type, due to their excellent capability to store elastic energy in microcavity which is made from high *Q* materials.[11] In the PnC domain, the periodicity of the elastic coefficients leads to the existence of phononic band gaps, in which the propagation of elastic wave is forbidden in any direction. The frequency range of the phononic band gap is dominated by the composition and geometry of the constitutive materials.[12,13] PnCs with well-engineered geometry have been demonstrated with several important properties such as band gaps,[14] band edge states,[15] and the ability to reduce thermal conductivity.[16] More recently, the 2D PnC slab configuration, in which the wave propagation is vertically confined within the two surfaces of the slab, has received much attention. By adding certain defects within the PnC structure, the confinement and control of elastic waves, such as elastic waveguides and mechanical resonators,[17–20] can be achieved. For example, PnCs with a line defect created can be the basis to form a waveguide[21,22] or a cavity-mode resonator in the form of a Fabry–Perot (FP) cavity structure;[23–25] Bloch-mode resonators can be formed by adding an extra row of scattering holes,[26] reducing the central three rows of scattering holes,[27] or introducing alternate defects[28,29] to the FP cavity structure.

In this work, we report the simultaneous improvement of *Q* and *Z* of silicon PnC MM resonators which are formed by patterning additional scattering holes to the conventional FP cavity, which is realised by completely removing two rows of scattering holes from the centre of an otherwise perfect 2D array of air-silicon PnC slab. By varying the radii of additionally patterned scattering holes in the original FP cavity, including 2 μm, 4 μm, and 6 μm, simultaneous improvement of the *Q* and *Z* can be experimentally shown, demonstrating its great potential to overcome the aforementioned trade-off between *Z* and *Q* in conventional resonators

a)Author to whom correspondence should be addressed. Electronic mail: elelc@nus.edu.sg

 © 2014 AIP Publishing LLC

[This article is copyrighted as indicated in the article. Reuse of AIP content is subject to the terms at: http://scitation.aip.org/termsconditions. Downloaded to] IP: 137.132.250.14 On: Thu, 06 Mar 2014 06:08:49

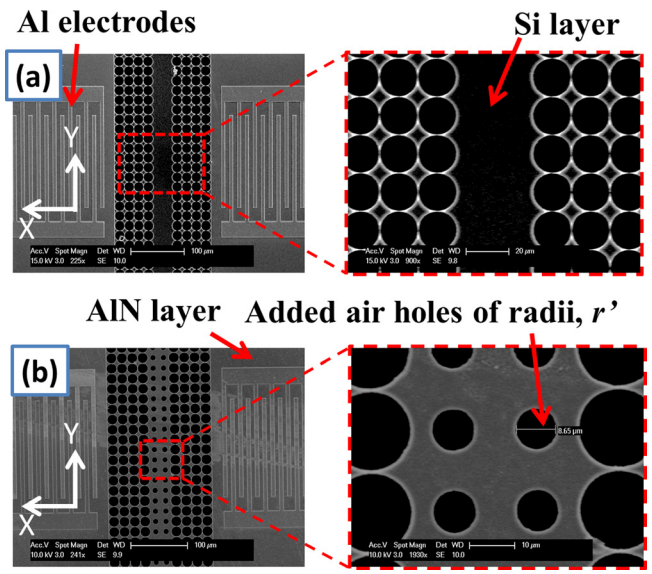

FIG. 1. SEM photographs of silicon PnC MM resonator (a) without additional scattering holes patterned in the FP cavity, (b) with additional scattering holes of radius, $r' = 4\,\mu$m, patterned in the FP cavity.

of piezoelectric type and capacitive type. In addition, Finite-Element-Modelling (FEM) approaches, which analyse the band diagrams of the defected FP cavities and the mode shapes of the structures at their respective supported modes, are in excellent agreement with the experimentally measured results.

II. RESONATOR DESIGN AND FABRICATION

Fig. 1(a) shows the SEM photograph of the silicon PnC MM resonator without additional scattering holes patterned in the FP cavity, i.e., two rows of scattering holes are completely absent at the centre of the air-hole square array; whereas Fig. 1(b) shows the SEM photograph of a typical silicon PnC MM resonator with additional scattering holes patterned. The areas enclosed by dashed red square are the areas to be zoomed in and the close-up views which show the central cavity region are depicted on the right side of Figs. 1(a) and 1(b), respectively. The post CMOS-compatible microfabrication process to realise the proposed silicon PnC MM resonators have been reported in our previous work.[26] On both sides of the central cavity region, there are four rows of scattering holes patterned, with inter-digit-transducer (IDT) electrodes formed by aluminium (Al) on both sides of the outer PnC structure. The IDTs, which consist of inter-digital Al electrodes on top of the piezoelectric aluminium nitride (AlN) layer, are capable of generating acoustic waves when AC signal is applied to the input IDT and converting the transmitted acoustic waves back to AC signal of the output IDT. As such, the effects on the transmitted acoustic waves by the central PnC region can be detected.

III. DEVICE CHARACTERIZATION AND DISCUSSIONS

The testing setups and testing procedures have also been reported in our previous work,[23,26] so they will not be repeated here. Fig. 2 shows the experimental frequency response spectra of the silicon PnC MM resonator (a) without additional scattering holes patterned in the FP cavity, (b) with additional scattering holes of radius $(r') = 2\,\mu$m patterned in the FP cavity. From the measurement results shown in Fig. 2, it can be noticed that when additional two rows of scattering holes are patterned into the otherwise pure FP cavity whereby two rows of scattering holes are completely absent, the resonant frequency (f) jumps from 158 MHz to 169.7 MHz, Q improves from 698 to 1017, whereas the insertion loss (IL) reduces from 15 dB down to 12 dB. As all the design parameters for these two silicon PnC MM resonators are the same except for the additional scattering holes patterned in the second design, the differences in the resonators' performance will be solely caused by the configurations of the central cavity region, i.e., the additionally patterned scattering holes in the central FP cavity.

Fig. 3(a) shows the band diagram, which depicts the modal frequencies against wave vector along the first irreducible Brillouin zone, of the pure PnC lattice structure where the lattice constant (a) is 18 μm, the thickness of the silicon slab (d) is 10 μm and the radius of the scattering holes (r) is 8 μm. The above geometric parameters are optimized in order to obtain a reasonably wide band gap in the frequency domain[30] under the limitation of our fabrication capability.[27] The band diagram is calculated by finite elements method described in detail in Ref. 23, by the combination of calculated eigenfrequencies obtained when sweeping the wave vector along the irreducible part of the first Brillouin zone. The optimized band diagram shown in Fig. 3(a) reveals that a band gap extends from 163 MHz to 186 MHz (the frequency range bounded by the two red lines), which means that no modes can be supported within this frequency range.

When additional two rows of scattering holes are patterned into the pure FP cavity, the cavity itself turns into a periodic structure with the same lattice constant (a) and the

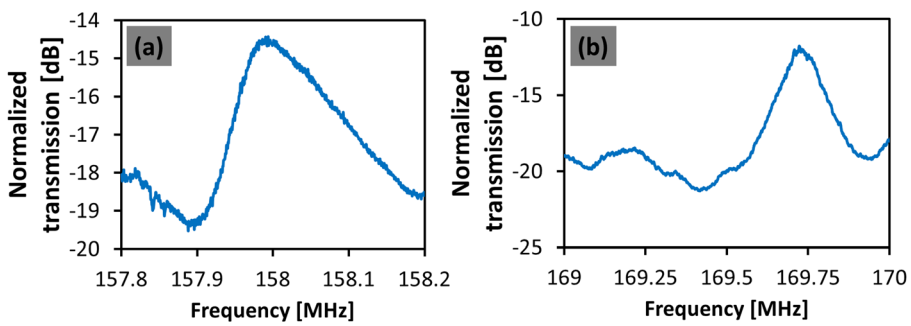

FIG. 2. Experimental frequency response spectra of the silicon PnC MM resonator (a) without additional scattering holes patterned in the FP cavity, (b) with additional scattering holes of radius, $r' = 2\,\mu$m, patterned in the FP cavity.

[This article is copyrighted as indicated in the article. Reuse of AIP content is subject to the terms at: http://scitation.aip.org/termsconditions. Downloaded to] IP: 137.132.250.14 On: Thu, 06 Mar 2014 06:08:49

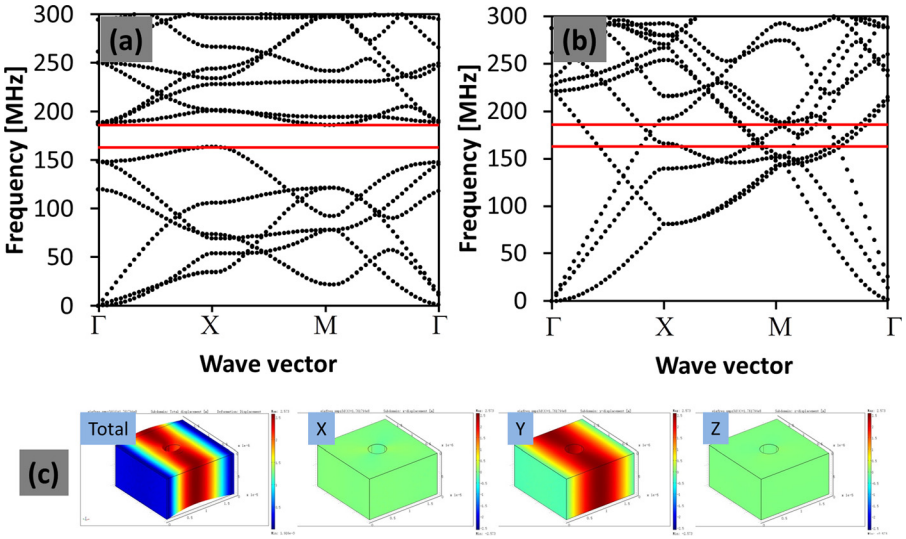

FIG. 3. FEM calculated band diagrams of the pure PnC lattice structures with (a) $a = 18\,\mu$m, $d = 10\,\mu$m, $r = 8\,\mu$m, (b) $a = 18\,\mu$m, $d = 10\,\mu$m, $r = 2\,\mu$m. (c) FEM calculated mode shapes, including total displacement and displacements in X, Y, Z directions, of the supported mode within the original band gap for the case of $r = 2\,\mu$m. The colour bar represents the displacement amplitude.

thickness (d) but with different hole radius (r) from the surrounding phononic structure. Therefore, the band diagram of the periodic structure in the central cavity region can be calculated using the method as described above. Fig. 3(b) depicts the band diagram for a pure PnC lattice structure with $a = 18\,\mu$m, $d = 10\,\mu$m, and $r = 2\,\mu$m. This is effectively the band diagram of the central cavity region of the silicon PnC MM resonator with additional holes of $r' = 2\,\mu$m. The frequency range bounded by the two red lines is the bandgap frequency range shown in Fig. 3(a), i.e., from 163 MHz to 186 MHz. From the calculated band diagram shown in Fig. 3(b), one can see that when additional scattering holes are patterned into the FP cavity, new modes can now be supported within the original band gap which does not support any modes. The frequencies of these modes fall into the original band gap of the pure PnC lattice structure when with $a = 18\,\mu$m, $d = 10\,\mu$m, and $r = 8\,\mu$m. Fig. 3(c) shows the mode shapes calculated by the aforementioned FEM method, in which the mode is corresponding to the frequency of resonance shown in Fig. 2(b). From both the total mode shape and the mode shapes in X, Y, Z directions, we can tell that for the mode which is supported within the original band gap and corresponds to the frequency of resonance shown in Fig. 2(b), the displacement polarization is concentrated in Y direction, with little or no polarization in X and Z directions.

In order for the physical scenarios of the entire phononic structure to be clearly seen, mode shapes, including displacement vector components in X, Y, and Z directions, of the whole phononic structures at their respective supported modes corresponding to the measured frequencies of resonance shown in Fig. 2, are simulated and shown in Fig. 4, with Fig. 4(a) showing the case of silicon PnC MM resonator without additional scattering holes patterned in the FP cavity and Fig. 4(b) showing the silicon PnC MM resonator with additional scattering holes of $r' = 2\,\mu$m patterned into the cavity. Fig. 4(a) shows the typical FP resonant modes, in which the elastic energy is concentrated at the central cavity region and distributed uniformly in the region, with the polarizations in X and Z directions. The mode is quite similar to the flexural mode of Lamb wave. On the other hand, when scattering holes are added into the centre of the FP cavity, the polarization change to Y direction, as shown in Fig. 4(b), with two kinds of oscillating modes appearing in the cavity at the same time. The first mode is evidenced by the largest displacement observed at the inner edges of the cavity, whereas the second mode is shown by the penetration of the elastic energy through the cavity. For convenience, we named the first mode the local-resonance (LR) mode and the second mode FP mode. Part of the incident elastic energy excites the LR mode which is analogous to the second localized mode reported in local resonant materials,[31] while another part of the energy excites the FP mode, which is evidenced by the penetration of the elastic energy through the cavity. The concentration of the displacement polarization in Y direction of the whole phononic structure echoes with the mode shapes of the central cavity region as depicted in

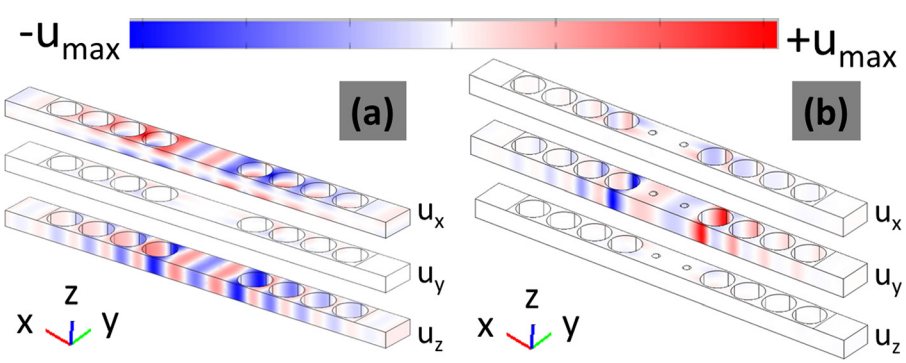

FIG. 4. FEM simulated mode shapes, including displacement vector components in X, Y, and Z directions, of the structures at their respective supported modes of the silicon PnC MM resonator (a) without additional scattering holes patterned in the FP cavity, (b) with additional scattering holes of radius, $r' = 2\,\mu$m, patterned in the FP cavity. The colour bar represents the displacement amplitude.

[This article is copyrighted as indicated in the article. Reuse of AIP content is subject to the terms at: http://scitation.aip.org/termsconditions. Downloaded to] IP: 137.132.250.14 On: Thu, 06 Mar 2014 06:08:49

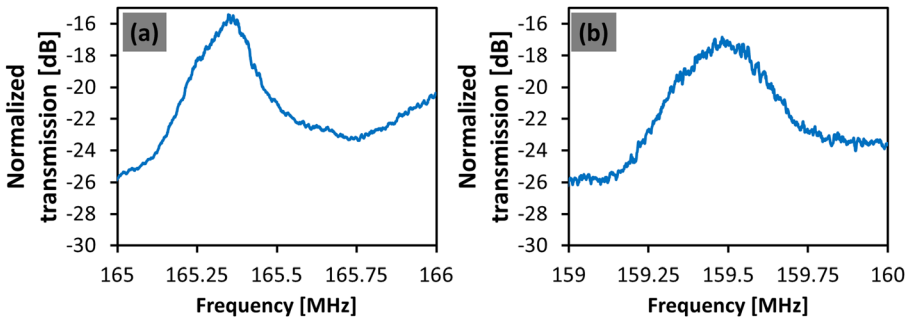

FIG. 5. Experimental frequency response spectra of the silicon PnC MM resonator with additional scattering holes of (a) $r' = 4\,\mu$m, (b) $r' = 6\,\mu$m, patterned in the FP cavity

Fig. 3(c), indicating that the Y polarization concentration of the whole phononic structure can actually be supported by the central cavity region.

From the energy point of view, the energy distributed along the structure is in a direct relationship with the displacement distribution, which can be extracted from the calculated mode shapes of the full phononic structure, because the energy associated with individual silicon atoms in the full structure is in a direct relationship with their displacement, when considering the individual silicon atom as a simple spring-mass system. The larger the displacement a particular nodal atom has, the higher the energy it is associated to. Therefore, the distribution of the stored elastic energy along the full structure can be estimated from the distribution of the modal displacement along the structures at their respective supported modes, which can be extracted from the calculated mode shapes of the full structure. For the silicon PnC MM resonator without additional scattering holes patterned in the FP cavity shown in Fig. 4(a), the mode shapes are not concentrated in the central FP cavity and the surrounding PnC region also gets displaced to some extent, indicating that the associated energy is not well confined within the central FP cavity, resulting in lower Q obtained due to larger amount of energy loss into the surrounding PnC region. On the other hand, for the silicon PnC MM resonator with additional scattering holes patterned into the FP cavity, the displacement vector components are mainly located at the central cavity region as illustrated in Fig. 4(b), the amount of energy loss is less due to good confinement of energy in the central cavity region, leading to higher Q obtained.

We further enlarge the radius of additionally patterned scattering holes (r') to 4 μm and 6 μm, with the normalized frequency response spectra shown in Figs. 5(a) and 5(b). As compared with the case of $r' = 2\,\mu$m, when r' is further increased to $4\,\mu$m, both f and Q drop, to a value of 165.32 MHz and 918, respectively, while IL increases to 15.41 dB. Nevertheless, the measured performance parameters are still better than the silicon PnC MM resonator without additional scattering holes patterned in the FP cavity. When r' is further enlarged to $6\,\mu$m, f drops further to 159.45 MHz but Q increases to 487, while IL also increases further to 17.51 dB, showing that the optimized resonant condition as obtained in the case of $r' = 2\,\mu$m is completely destroyed.

Figs. 6(a) and 6(b) depict the band diagrams for a pure PnC lattice structure with $r = 4\,\mu$m and $r = 6\,\mu$m, respectively, which essentially reveal the band diagrams of the

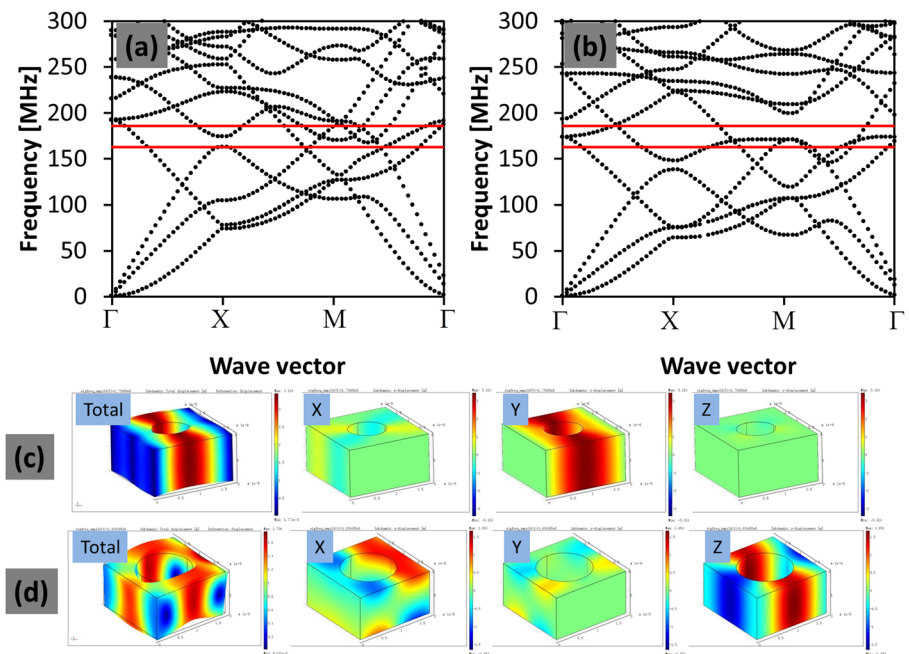

FIG. 6. (a),(b) FEM calculated band diagram of the pure PnC with (a) $a = 18\,\mu$m, $d = 10\,\mu$m, $r = 4\,\mu$m, (b) $a = 18\,\mu$m, $d = 10\,\mu$m, $r = 6\,\mu$m. (c),(d) FEM calculated mode shapes, including total displacement and displacements in X, Y, Z directions, of the supported mode within the original band gap for (c) $r = 4\,\mu$m, (d) $r = 6\,\mu$m. The colour bar represents the displacement amplitude.

[This article is copyrighted as indicated in the article. Reuse of AIP content is subject to the terms at: http://scitation.aip.org/termsconditions. Downloaded to] IP: 137.132.250.14 On: Thu, 06 Mar 2014 06:08:49

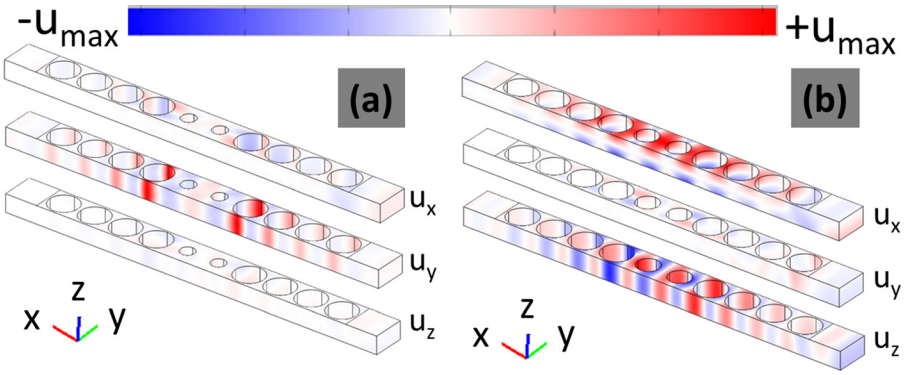

FIG. 7. FEM simulated mode shapes, including displacement vector components in X, Y, and *Z* directions, of the structures at their respective supported modes of the silicon PnC MM resonator with additional scattering holes of (a) $r' = 4\,\mu$m, (b) $r' = 6\,\mu$m. The colour bar represents the displacement amplitude.

central cavity regions of the silicon PnC MM resonators with additional scattering holes of $r' = 4\,\mu$m and $r' = 6\,\mu$m patterned in the FP cavity, respectively. Still, the regions bounded by the two sets of red lines are the band-gap frequency range shown in Fig. 3(a), i.e., from 163 MHz to 186 MHz; Figs. 6(c) and 6(d) show the mode shapes of the new modes which correspond to the frequency of resonances in Figs. 5(a) and 5(b), respectively and are supported within the original band gap. From the calculated mode shapes, it can be seen that the displacement polarization is concentrated in Y direction for the supported mode corresponding to the frequency of resonance for the case of $r' = 4\,\mu$m, as shown in Fig. 5(a). With further increment of r' to 6 μm, the displacement polarization is concentrated in X and *Z* directions for the supported mode corresponding to the frequency of resonance in Fig. 5(b). These two modes also echo with the mode shapes of the full phononic structures which will be discussed in detail in the next paragraph.

Figs. 7(a) and 7(b) show the mode shapes of the full phononic structure of silicon PnC MM resonators with additional scattering holes of $r' = 4\,\mu$m and $r' = 6\,\mu$m patterned into the cavity, respectively. Again, for the case of Fig. 7(a), the displacement components are concentrated at the central cavity region, showing better ability in energy confinement which subsequently leads to higher *Q* obtained. On the contrary, the displacement components for the case of Fig. 7(b) are poorly confined within the cavity and leak to the surrounding PnC region, leading to lower *Q* obtained. From the viewpoint of the polarization concentration of the full phononic structure, the silicon PnC MM resonator with additional scattering holes of $r' = 4\,\mu$m patterned in the FP cavity has its polarization concentrated in Y direction as shown in Fig. 7(a), indicating the coexistence of both the LR mode and the FP mode, i.e., the mode evidenced by the largest displacement at the inner edges of the cavity, and the mode shown by the penetration of the elastic energy through the cavity, respectively, which is similar to the case of $r' = 2\,\mu$m as shown in Fig. 4(b). Upon further increment of r' to 6 μm, the mode turns back to the typical FP mode with its polarization concentrated in X and *Z* directions.

From the FEM simulated mode shapes of the full phononic structure, the acoustic wave's speed in the central cavity region can be calculated by the equation $v = f\lambda$, whereby v is the acoustic wave's speed in the central cavity region, f is the resonant frequency, λ is the wavelength of the acoustic waves and given by dividing the length of the cavity (L) by the number of periods of waves within the central cavity. For all the silicon PnC MM resonators reported in this work, as two rows of scattering holes are removed, the length of the cavity can be calculated by $L = 3a - 2r$, with a being the lattice constant and r being the radius of the scattering holes at the PnC region surrounding the central cavity region. As mentioned previously, a and r are optimized to be 18 μm and 8 μm, respectively, for the PnC lattice structures in this work. Therefore, the length of cavity (L) for the silicon PnC MM resonators with two rows of scattering holes removed from the centre of the PnC region reported in this work turns out to be 38 μm.

For the silicon PnC MM resonator without additional scattering holes patterned in the FP cavity as shown in Fig. 4(a), there are 1.5 periods of wave within the cavity. Therefore, the acoustic wave's speed in the central cavity region is $v = f\lambda = 158 \times 38/1.5 = 4003$ m/s. Similarly, the acoustic wave's speed in the central cavity region for the silicon PnC MM resonator with additional scattering holes of $r' = 2\,\mu$m [Fig. 4(b)], $r' = 4\,\mu$m [Fig. 7(a)], $r' = 6\,\mu$m [Fig. 7(b)] can be calculated to be 6449 m/s, 4188 m/s, and 3030 m/s, respectively.

The experimentally measured results, together with the other three calculated results, i.e., the *f*-*Q* product, *Z*, as well as the acoustic wave's speed in the central cavity region, of all the silicon PnC MM resonators reported in this paper are summarized in Table I below. The case of $r' = 0\,\mu$m is essentially the silicon PnC MM resonator without additional scattering holes patterned in the FP cavity.

In Table I, the *f*-*Q* products are calculated by multiplying the measured f with the measured Q, while the value of equivalent Z can be extracted by Eq. (1)[32]

$$Z = 50 \times 10^{IL/20}. \quad (1)$$

TABLE I. Measured and calculated results of silicon PnC MM resonators reported in this work.

	r′(μm)			
Performance parameters	0	2	4	6
f (MHz)	158	169.7	165.32	159.45
Q	698	1017	918	487
IL (dB)	15	12	15.41	17.51
f-*Q* product (Hz)	1.1×10^{11}	1.73×10^{11}	1.52×10^{11}	0.78×10^{11}
Z (Ω)	281	199	294	375
v (m/s)	4003	6449	4188	3030

[This article is copyrighted as indicated in the article. Reuse of AIP content is subject to the terms at: http://scitation.aip.org/termsconditions. Downloaded to] IP: 137.132.250.14 On: Thu, 06 Mar 2014 06:08:49

From Table I, one can notice that from the case of $r' = 2\,\mu$m to the case of $r' = 6\,\mu$m, Q drops while Z increases. This means that both performance parameters (Q and Z) degrade when r' is increased from 2 μm to 6 μm. Therefore, if one notes the performance parameters backwards from the case of $r' = 6\,\mu$m to the case of $r' = 2\,\mu$m, the Q and Z improve simultaneously, instead of improving one at the expense of degrading the other as in the case of capacitive-type and piezoelectric-type devices. Therefore, we can see the great potential of silicon PnC MM resonators to overcome the aforementioned trade-off between Q and Z.

It is worth to note that the acoustic wave's speed in the central cavity region is in a direct relationship with the obtained Q, i.e., the higher the wave's speed, the higher the Q obtained. For example, the case of $r' = 2\,\mu$m has the highest acoustic wave's speed in the central cavity region of 6449 m/s, it also has the highest Q of 1017 obtained; the case of $r' = 6\,\mu$m has the lowest acoustic wave's speed in the central cavity region of 3030 m/s, it also has the lowest Q of 487 obtained. This can be explained by considering the acoustic wave's speed along the lateral direction (Y direction) in the central cavity region. If one views the central cavity region of the silicon PnC MM resonators reported in this work along the Y direction, the central cavity region is effectively a waveguide, with the top end and the bottom end left open. Therefore, when the acoustic wave's speed in the central cavity region is high, the acoustic wave will be bounced constantly by the two edges of the central cavity at a high rate since the length of the cavity is constant. Therefore, the Y component of the acoustic wave's speed in the central cavity region is insignificant as compared to its X component. As a result, the amount of energy loss through leaking from the two open ends of the waveguide along Y direction is small, rendering higher Q obtained. On the other hand, when the acoustic wave's speed in the central cavity region is low, the group velocity in Y direction is fast, leading to larger amount of energy leakage through the two open ends of the waveguide. Consequently, the Q obtained is lower.

When considering the IL together with the Q, both performance parameters (Q and Z) degrade when r' is increased from 2 μm to 6 μm. On the other way of saying, both parameters can be improved at the same time, showing great potential of silicon PnC MM resonator overcome the aforementioned trade-off between Q and Z. This is different from the cases of conventional capacitive-type and piezoelectric-type devices, whereby one parameter can be improved at the expense of degrading the other.

IV. CONCLUSION

In this paper, we report the experimental evidence which shows that silicon PnC MM resonators with additional scattering holes patterned in the central FP resonant cavity region can have Q and Z improved at the same time, by varying the radii of the additional scattering holes to be $r' = 6\,\mu$m, $r' = 4\,\mu$m, and $r' = 2\,\mu$m. Experimentally measured results, which include f, Q, as well as IL, together with calculated results including f-Q product, Z and v, of the fabricated silicon PnC MM resonators, are discussed by calculating the band diagrams of the central cavity region, analysing the mode shapes of the central cavity region as well as the full phononic structure at their respective supported modes. The proposed resonators show great potential in overcoming the aforementioned trade-off between the Q and Z in traditional capacitive-type and piezoelectric-type devices.

ACKNOWLEDGMENTS

The authors acknowledge the support from the Science and Engineering Research Council (SERC) of Agency for Science, Technology and Research (A*STAR), Singapore, under Grant No. SERC 1220103064 (R263000A56305); and Faculty Research Committee (FRC) Fund (R263000692112) from the National University of Singapore; and National Science Council NSC 101-2221-E-018-013, Taiwan.

[1]H. M. Lavasani, R. Abdolvand, and F. Ayazi, in *Proceedings of IEEE Custom Integrated Circuits Conference* (IEEE, 2007), p. 599.
[2]S. Ryder, K. B. Lee, X. F. Meng, and L. W. Lin, Sens. Actuators, A **114**, 135 (2004).
[3]K. Wang, A. C. Wong, and C. T. C. Nguyen, J. Microelectromech. Syst. **9**, 347 (2000).
[4]S. Pourkamali, A. Hashimura, R. Abdolvand, G. K. Ho, A. Erbil, and F. Ayazi, J. Microelectromech. Syst. **12**, 487 (2003).
[5]J. E. Y. Lee and A. A. Seshia, Sens. Actuators, A **156**, 28 (2009).
[6]G. K. Ho, R. Abdolvand, A. Sivapurapu, S. Humad, and F. Ayazi, J. Microelectromech. Syst. **17**, 512 (2008).
[7]G. Piazza, P. J. Stephanou, and A. P. Pisano, J. Microelectromech. Syst. **15**, 1406 (2006).
[8]G. Piazza, R. Abdolvand, G. K. Ho, and F. Ayazi, Sens. Actuators, A **111**, 71 (2004).
[9]C. T. C. Nguyen, IEEE Trans. Ultrason. Ferroelectr. Freq. Control **54**, 251 (2007).
[10]G. Piazza, P. J. Stephanou, and A. P. Pisano, J. Microelectromech. Syst. **16**, 319 (2007).
[11]R. H. Olsson and I. El-Kady, Meas. Sci. Technol. **20**, 012002 (2009).
[12]M. S. Kushwaha, P. Halevi, L. Dobrzynski, and B. Djafarirouhani, Phys. Rev. Lett. **71**, 2022 (1993).
[13]M. Sigalas and E. N. Economou, Solid State Commun. **86**, 141 (1993).
[14]R. Martinezsala, J. Sancho, J. V. Sanchez, V. Gomez, J. Llinares, and F. Meseguer, Nature **378**, 241 (1995).
[15]C. Y. Qiu and Z. Y. Liu, Appl. Phys. Lett. **89**, 063106 (2006).
[16]P. E. Hopkins, C. M. Reinke, M. F. Su, R. H. Olsson, E. A. Shaner, Z. C. Leseman, J. R. Serrano, L. M. Phinney, and I. El-Kady, Nano Lett. **11**, 107 (2011).
[17]J. O. Vasseur, A. C. Hladky-Hennion, B. Djafari-Rouhani, F. Duval, B. Dubus, Y. Pennec, and P. A. Deymier, J. Appl. Phys. **101**, 114904 (2007).
[18]A. Khelif, A. Choujaa, B. Djafari-Rouhani, M. Wilm, S. Ballandras, and V. Laude, Phys. Rev. B **68**, 214301 (2003).
[19]M. Oudich, M. B. Assouar, and Z. Hou, Appl. Phys. Lett. **97**, 193503 (2010).
[20]Y. W. Gu, X. D. Luo, and H. R. Ma, J. Appl. Phys. **105**, 044903 (2009).
[21]A. Khelif, S. Mohammadi, A. A. Eftekhar, A. Adibi, and B. Aoubiza, J. Appl. Phys. **108**, 084515 (2010).
[22]R. H. Olsson, I. F. El-Kady, M. F. Su, M. R. Tuck, and J. G. Fleming, Sens. Actuators, A **145**, 87 (2008).
[23]N. Wang, J. M. Tsai, F. L. Hsiao, B. W. Soon, D. L. Kwong, M. Palaniapan, and C. Lee, IEEE Electron Device Lett. **32**, 821 (2011).
[24]S. Mohammadi, A. A. Eftekhar, W. D. Hunt, and A. Adibi, Appl. Phys. Lett. **94**, 051906 (2009).
[25]S. Mohammadi, A. A. Eftekhar, R. Pourabolghasem, and A. Adibi, Sens. Actuators, A **167**, 524 (2011).
[26]N. Wang, J. M. L. Tsai, F. L. Hsiao, B. W. Soon, D. L. Kwong, M. Palaniapan, and C. Lee, J. Microelectromech. Syst. **21**, 801 (2012).

[This article is copyrighted as indicated in the article. Reuse of AIP content is subject to the terms at: http://scitation.aip.org/termsconditions. Downloaded to] IP: 137.132.250.14 On: Thu, 06 Mar 2014 06:08:49

[27]N. Wang, F. L. Hsiao, J. M. Tsai, M. Palaniapan, D. L. Kwong, and C. Lee, J. Micromech. Microeng. **23**, 065030 (2013).
[28]N. Wang, F.-L. Hsiao, M. Palaniapan, and C. Lee, Appl. Phys. Lett. **99**, 234102 (2011).
[29]N. Wang, F. L. Hsiao, J. M. Tsai, M. Palaniapan, D. L. Kwong, and C. Lee, J. Appl. Phys. **112**, 024910 (2012).
[30]S. Mohammadi, A. A. Eftekhar, A. Khelif, H. Moubchir, R. Westafer, W. D. Hunt, and A. Adibi, Electron. Lett. **43**, 898 (2007).
[31]Z. Y. Liu, X. X. Zhang, Y. W. Mao, Y. Y. Zhu, Z. Y. Yang, C. T. Chan, and P. Sheng, Science **289**, 1734 (2000).
[32]S. Pourkamali, G. K. Ho, and F. Ayazi, IEEE Trans. Electron Devices **54**, 2017 (2007).

[This article is copyrighted as indicated in the article. Reuse of AIP content is subject to the terms at: http://scitation.aip.org/termsconditions. Downloaded to] IP: 137.132.250.14 On: Thu, 06 Mar 2014 06:08:49